Neuron, Vol. 35, 521–533, August 1, 2002, Copyright ©2002 by Cell Press

Spillover of Glutamate onto Synaptic AMPA Receptors Enhances Fast Transmission at a Cerebellar Synapse

David A. DiGregorio,[1] Zoltan Nusser,[2] and R. Angus Silver[1]
[1]Department of Physiology
University College London
Gower Street
London, WC1E 6BT
United Kingdom
[2]Laboratory of Cellular Neurophysiology
Institute of Experimental Medicine
Hungarian Academy of Sciences
Szigony Street 43
1083 Budapest
Hungary

Summary

Diffusion of glutamate from the synaptic cleft can activate high-affinity receptors, but is not thought to contribute to fast AMPA receptor-mediated transmission. Here, we show that single AMPA receptor EPSCs at the cerebellar mossy fiber-granule cell connection are mediated by both direct release of glutamate and rapid diffusion of glutamate from neighboring synapses. Immunogold localization revealed that AMPA receptors are located exclusively in postsynaptic densities, indicating that spillover of glutamate occurs between synaptic contacts. Spillover currents contributed half the synaptic charge and exhibited little trial-to-trial variability. We propose that spillover of glutamate improves transmission efficacy by both increasing the amplitude and duration of the EPSP and reducing fluctuations arising from the probabilistic nature of transmitter release.

Introduction

Fast excitatory synaptic transmission in the central nervous system (CNS) is classically thought to occur at synaptic contacts or active zones (AZs) where glutamate is released from presynaptic specializations directly onto ionotropic receptors located in postsynaptic densities (PSDs). This "point-to-point" communication allows precise, spatially localized signaling between neurons and storage of information as independent synaptic weights. However, diffusion of glutamate out of the synaptic cleft has recently been shown to activate both high-affinity metabotropic (Mitchell and Silver, 2000; Scanziani et al., 1997) and NMDA receptors (Asztely et al., 1997; Isaacson, 1999) at neighboring synapses. Glutamate spillover onto low-affinity AMPA receptors (AMPARs) has only been demonstrated following tetanic stimulation of multiple input fibers in cerebellar cortex (Carter and Regehr, 2000). But, it is unclear whether glutamate released from neighboring synapses contributes to AMPAR activation during a single excitatory postsynaptic current (EPSC).

Correspondence: a.silver@ucl.ac.uk

The rapidly decaying component of AMPAR EPSCs can result from receptor deactivation following a brief glutamate transient (Hestrin, 1992; Silver et al., 1996a). The presence of slowly decaying components in some synaptic currents indicates that significant levels of glutamate can persist in the synaptic cleft for tens of milliseconds (Barbour et al., 1994; Neher and Sakaba, 2001; Silver et al., 1996a). Such glutamate concentrations could be produced by spillover of glutamate or its slow clearance from the synaptic cleft following release from a single vesicle. It is also possible that slow current components arise from the activation of receptors in the perisynaptic region (Chen and Diamond, 2002). Recent modeling studies have cast doubt on whether synaptic AMPARs can be activated by spillover, given diffusion distances and the extracellular volume fraction of typical brain tissue (Barbour, 2001; Barbour and Hausser, 1997; Rusakov, 2001). Nevertheless, the observations that receptor occupancy (Silver et al., 1996b) and the EPSC time course (Mennerick and Zorumski, 1995; Otis et al., 1996; Silver et al., 1996b, 1998; Trussell et al., 1993) are dependent on release probability suggest that AMPARs can be activated by glutamate released at neighboring AZs connected to the same cell. However, similar changes in EPSC waveform at the cerebellar climbing fiber synapse have been interpreted as a change in the number of quanta released per release site (Wadiche and Jahr, 2001) rather than arising from glutamate spillover. Without direct resolution of spillover-mediated AMPAR EPSCs, the level of interaction between AZs and, thus, the contribution of spillover to fast synaptic transmission, remains unclear.

We examined whether glutamate spillover contributes to fast EPSCs by taking advantage of the unique anatomy of the excitatory mossy fiber (MF) to granule cell (GC) synapse, a connection where the same presynaptic terminal diverges onto many different postsynaptic cells within a synaptic glomerular structure (Eccles et al., 1967). The small size and compact morphology of the GC also allowed EPSC recordings of exceptional temporal resolution (Silver et al., 1992). We found that single AMPAR EPSCs have two distinct components: conventional fast-rising currents and novel slow-rising currents. We demonstrate that the slow-rising currents arise from synaptic AMPARs activated by glutamate released from synapses connected to neighboring GCs.

Results

Identification of Slow-Rising Non-NMDA Receptor EPSCs

We investigated fast excitatory synaptic transmission at the MF-GC synapse in acute slices of cerebellum from 25-day-old (postnatal day [P]25) rats at physiological temperature (37°C). At this age, the anatomical development of the glomerular structure is nearly complete (Hamori and Somogyi, 1983). Single MF inputs were activated using extracellular stimulation of the GC layer as previously described (Silver et al., 1996b), and NMDA,

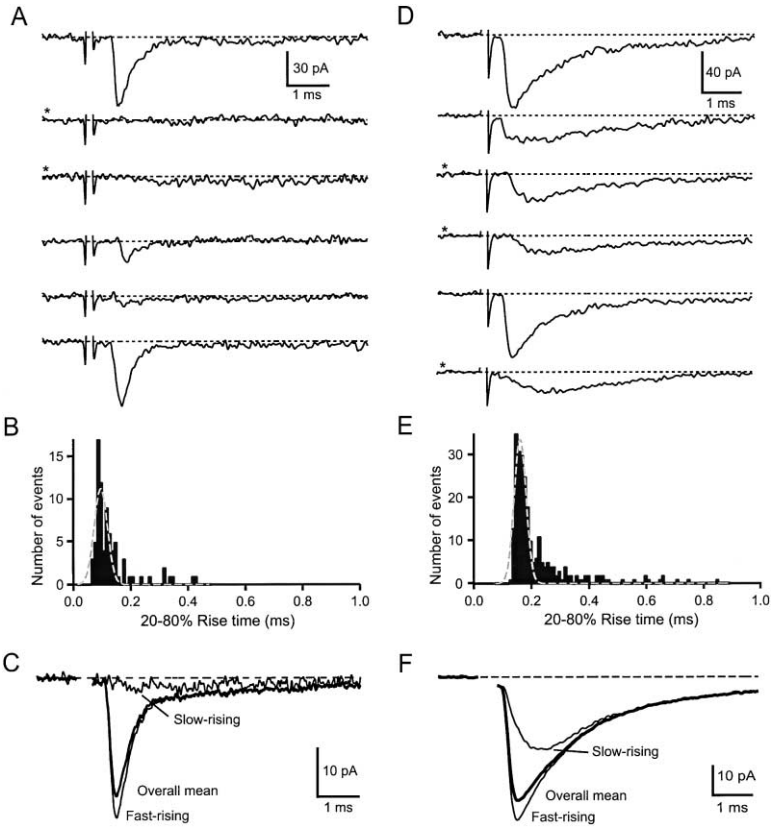

Figure 1. Identification of Individual Slow-Rising EPSCs

(A) Individual EPSCs recorded from a MF-GC connection in which events were either fast-rising and -decaying or apparent synaptic failures (*).

(B) The rise time distribution fitted with a Gaussian function (dashed line).

(C) Synaptic failures, as well as events slower than 5 × SD + the mean of the Gaussian fit (0.21 ms) and lacking a fast-rising component, were grouped and averaged (slow-rising, n = 13 events). The remaining events were averaged and denoted as fast-rising (10%–90% rise time [RT] = 0.18 ms, n = 79). The overall mean is the average of all the evoked events for this cell (RT = 0.18 ms).

(D) Individual EPSCs recorded from a different cell in which both fast-rising and slow-rising (*) events were recorded.

(E) Rise time histogram and Gaussian fit (dashed line) of all events from the connection shown in (D).

(F) Events from (D) were separated, averaged, and labeled as in (C) (fast-rising, RT = 0.24 ms, n = 300; slow-rising, RT = 0.57 ms, n = 18; overall mean, RT = 0.26 ms). Individual EPSCs are presented with a filter cutoff frequency of 4.5 kHz.

$GABA_A$, and glycine receptors were blocked with selective antagonists to isolate non-NMDA mediated EPSCs. Figure 1 shows examples of EPSCs recorded from two different MF-GC synaptic connections. One of them (Figures 1A–1C) exhibited fast-rising synaptic currents or apparent "failures," similar to that shown previously in P12 animals (Silver et al., 1996a). The EPSCs for the other cell (Figures 1D–1F), which are more characteristic for this age, had both fast-rising events as well as slow-rising non-NMDA EPSCs. The rise time distribution of both inputs had unimodal peaks (similar to Geiger et al., 1997; Silver et al., 1996b) below 200 μs, but the cell in Figure 1D had a larger proportion of the events with slow rise times (Figures 1B and 1E).

To characterize further the slow-rising events, we separated EPSCs into two groups based on the speed of their rising phase (see Experimental Procedures; note that failures were included in the slow-rising group). The cell shown in Figures 1A–1C had both an overall and a fast-rising mean with similar rise times. The decay was predominantly fast with a small-amplitude slow tail, similar to that observed in P12 rats (Silver et al., 1996a). The amplitude of the mean slow-rising EPSC was small, consistent with all but one of the events being failures. For the cell shown in Figures 1D–1F, both the overall and fast-rising means also exhibited similar rise times that were comparable to the first cell. The mean slow-rising EPSC was much larger than that of the first cell yet was still smaller than its overall and fast-rising means, although this cell exhibited no failures (Figure 1F). Of the 86 connections tested, 71 exhibited isolated slow-rising currents, which occurred in 17% of trials. Their mean amplitude was always smaller than the mean fast-rising EPSC (slow:fast amplitude ratio is 0.34 ± 0.17, mean ± SD). For those cells with a small stimulus artifact, the average 10%–90% rise time was 0.19 ± 0.03 ms (mean ± SD, n = 65 cells) for mean fast-rising EPSCs and 0.81 ± 0.39 ms (n = 50) for mean slow-rising EPSCs. The decay of the slow-rising EPSC lacked a fast component, but was similar to both the overall and fast-rising means at late times (≥5 ms; Figure 1F). The observation that the cell with a prominent slow-rising current was associated with a slowly decaying overall mean EPSC was born out across many cells, which exhibited a significant correlation between their weighted decay (see Figure 2A, legend) and slow:fast amplitude ratio (n = 71 cells; Figure 2B). This suggests that the slow-rising component is a major determinant of the non-NMDA EPSC waveform. Moreover, the weighted decay can be used as a measure of the relative contribution of the slow-rising current to the mean EPSC.

Isolation of the Fast Component of Non-NMDA Receptor EPSCs

We examined whether fast-rising and -decaying current components, similar to those in Figure 1C, were also present in cells with slow-rising currents. To do this, we selected fast-rising currents at low release probability, thereby increasing the chance of observing this component in isolation. The weighted decay of the mean fast-rising EPSC became faster when release probability was reduced by lowering the extracellular calcium concentration ($[Ca^{2+}]_e$; 2.9 to 1.6 ms; Figure 2C) and no longer followed the same decay time course as the mean slow-

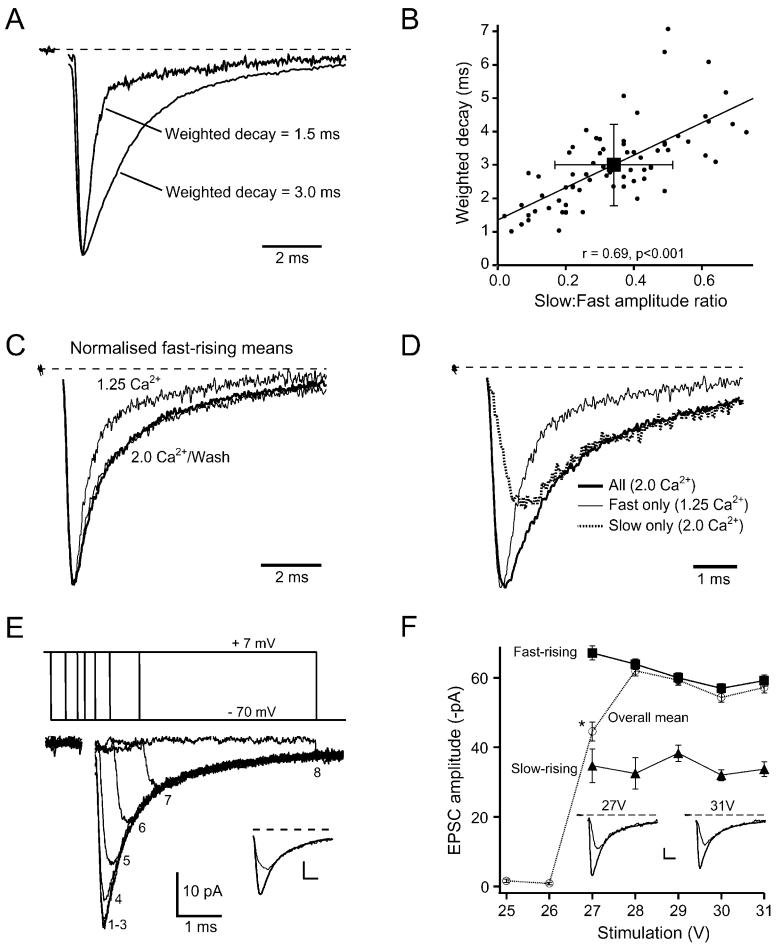

Figure 2. Slow-Rising Events Shape the Mean EPSC, Are Distinct from Fast-Rising Events, and Do Not Result from Dendritic Filtering

(A) Normalized mean EPSC waveforms from the cells in Figure 1 show a slower decay for the connection with large, slow-rising EPSCs. Weighted decay was calculated by normalizing the peak of the EPSC to one and integrating for 20 ms from the start of the EPSC.

(B) Correlation plot of the weighted decay versus the slow:fast amplitude ratio ($n = 71$ cells). The square is the mean and SD (error bars) of the weighted decay (3.0 ± 1.2 ms) and amplitude ratio. Solid line is a linear fit to the data points with a y-intercept of 1.35 ms.

(C) Mean fast-rising EPSCs in 2 mM $[Ca^{2+}]_e$ (thick trace), 1.25 mM (thin trace), and back to 2 mM (wash).

(D) Time course of the overall mean EPSC (thick trace), mean slow-rising EPSC recorded in 2 mM $[Ca^{2+}]_e$, and the mean fast-rising EPSC recorded in 1.25 $[Ca^{2+}]_e$ (thin trace) from the same cell. The fast-rising EPSC was scaled to the peak of the mean EPSC.

(E) A voltage jump experiment where EPSCs were elicited when repolarizing the cell from 7 to –70 mV at eight different times. Each trace is an average of 75 events and was calculated from a subtraction with and without an extracellular stimulus. The traces are numbered (one to eight) in accordance with each of the eight repolarization times (from start of blanked region): −2, −1, −0.2, 0.2, 1, 2, 4, and 16 ms, respectively. Inset, the overall mean (thick trace) and mean slow-rising (thin trace) EPSC from this cell.

(F) EPSC peak amplitudes recorded as a function of stimulus intensity showing that like the overall mean EPSC (open circles), the amplitude of mean slow-rising EPSC (triangles) and mean fast-rising EPSC (squares) occurred at the same stimulus voltage in an all-or-none manner. The asterisk identifies the overall mean EPSC recorded at threshold for fiber stimulation where we observed failures that were not present at higher stimulation intensities, thus resulting in a lower mean peak amplitude at this voltage. Insets, the mean fast-rising EPSC (thick trace) and mean slow-rising EPSC (thin trace) at 27 and 31 V.

Scale bar: 10 pA and 1 ms in (E) and (F).

rising EPSC at late times (Figure 2D). The average weighted decay of the fast-rising currents was reduced from 2.3 ± 0.2 ms in 2 mM $[Ca^{2+}]_e$ to 1.4 ± 0.1 ms in low $[Ca^{2+}]_e$ (1.0–1.25 mM; $p < 0.001$; $n = 13$ cells); this was reversible in the seven cells tested. The weighted decay of the isolated fast-rising current in low $[Ca^{2+}]_e$ is similar to that for the cell in Figure 2A and to the extrapolation of the linear regression in Figure 2B (1.4 ms). These results confirm that non-NMDA EPSCs are composed of independently occurring, conventional fast-rising and -decaying currents as well as novel slow-rising and -decaying currents (Figure 2D), which are revealed when the fast-rising currents fail. The slow-rising non-NMDA current component is reminiscent of spillover currents mediated by high-affinity α_6-containing $GABA_A$ receptors at the Golgi cell-GC synapse (Rossi and Hamann, 1998), albeit with a ~50-fold faster time course.

Slow-Rising Currents Do Not Arise from Dendritic Filtering

If the slow component of the EPSC is caused by dendritic filtering, then the EPSC time course would extend beyond the time when the synaptic conductance is active. However, if the synapse is well voltage clamped, the EPSC and synaptic conductance waveform would be similar. We examined whether slow-rising currents arose from dendritic filtering using the voltage-jump technique (Hausser and Roth, 1997). All the remaining current was recovered when the voltage was stepped from near the reversal potential to a hyperpolarized potential, even at late times, indicating that the synaptic conductance is active throughout the EPSC (Figure 2E; $n = 5$ cells). These data confirm that in P25 GCs, the synaptic currents are well voltage clamped under our conditions and rule out the possibility that the slow-rising non-NMDA currents arise from electrically remote sites on the dendrite or from electrically coupled cells.

Fast- and Slow-Rising Currents Arise from the Same Mossy Fiber Terminal

We next investigated whether slow-rising EPSCs arose from the same MF as the fast-rising EPSCs or from glutamate released from neighboring MFs. We found that both fast- and slow-rising EPSCs were elicited at the same stimulus voltage ($n = 5$ cells; Figure 2F). Moreover,

increasing the stimulation voltage did not increase the amplitude of either current. Since an MF is only thought to make a single connection to a granule cell (Eccles et al., 1967), these results suggest that fast- and slow-rising currents arise from the activation of the same terminal. Moreover, both current components were blocked by 500 nM tetrodotoxin, suggesting that AP invasion of the MF terminal is necessary to elicit both current types ($n = 5$; data not shown).

Synaptic AMPARs Mediate the Slow-Rising Current

High-affinity kainate receptors are present at the soma of cerebellar GCs (Smith et al., 1999) and mediate slow synaptic currents in cerebellar Golgi cells (Bureau et al., 2000). We tested whether kainate receptors underlie the slow-rising EPSC in GCs by using selective AMPAR antagonists. Application of 50 μM GYKI 53655 ($n = 5$ cells) or 100 μM SYM2206 ($n = 3$), concentrations that block AMPARs but attenuate kainate currents by less than 20% (Li et al., 1999; Smith et al., 1999; Wilding and Huettner, 1995), abolished both fast- and slow-rising currents (Figure 3A), indicating that both components of the EPSC are mediated by AMPARs.

Slow-rising currents could arise from activation of AMPARs located within AZs or in the extrasynaptic membrane. We therefore investigated the spatial distribution of AMPARs expressed in GCs with postembedding electron microscopic immunogold labeling. We visualized AMPARs using a GluR2/3/4c polyclonal antibody. Each of the 28 asymmetric synaptic junctions between MFs and GC dendrites examined had at least one gold particle (range: one through nine) with a mean of 4.7 ± 2.0 (Figure 3B). The density of gold particles at MF-GC synapses was nearly 100-fold higher (430 ± 26 particles/μm^2, $n = 28$ synapses in 12 images from 3 animals) than on mitochondria, which were used to determine the nonspecific labeling density (6.2 ± 3.4 particles/μm^2, $p < 0.001$). The density of gold particles on the extrasynaptic plasma membrane (3.0 ± 1.2 particles/μm^2) was not significantly different from that on mitochondria ($p = 0.24$, unpaired t test; Figure 3C).

In a second set of experiments, we further enhanced the sensitivity of the technique by using a mixture of the anti-GluR2/3/4c antibody and a polyclonal antibody against all AMPAR subunits (anti-pan-AMPAR; Nusser et al., 1998). In the tissue with the highest specific labeling, the synaptic gold particle density increased by 66% (from 452 ± 164 particles/μm^2, $n = 16$, to 751 ± 253 particles/μm^2, $n = 10$). The extrasynaptic gold particle density was increased by 170% (to 8.0 particles/μm^2), which was almost identical to the increase in the nonspecific labeling observed over mitochondria, to 180% (17.5 particles/μm^2). Thus, despite the increased sensitivity (64% after background subtraction) and specificity for all AMPAR subunits, the labeling of the extrasynaptic membrane remained insignificant. These results show that in cerebellar granule cells all detectable AMPARs are located in PSDs.

We examined electron micrographs of rat cerebellar glomeruli to estimate the mean distance between synaptic contacts. Nearest neighbor analysis of PSDs from 2D sections gave a distribution with a mean distance between PSDs of 0.77 μm (edge-to-edge; Figure 3D), similar to another preparation where spillover is theoretically possible (0.7 μm, Otis et al., 1996). This approach is likely to overestimate inter-PSD distance, as closer sites may be present in different section planes. We found little evidence for the presence of glial cell processes close to the release sites, consistent with the idea that glial cells are restricted to the periphery, forming an external sheath around the glomerular structure (Eccles et al., 1967).

Intersynaptic Spillover Hypothesis

Our working hypothesis for AMPAR-mediated synaptic transmission at the MF-GC synaptic connection is illustrated in Figure 3E. Fast-rising EPSCs result from glutamate released at those synaptic contacts connected to the GC from which we recorded. Diffusion of glutamate from neighboring AZs connected to up to 50 other GCs (Jakab and Hamori, 1988) contributes a slow-rising and slow-decaying current that underlies the slow decay of the fast-rising EPSC. When direct release fails (see glomerulus on right), this slow-rising and -decaying "spillover" current is revealed in isolation. In the following sections, we test this hypothesis.

Kynurenic Acid Preferentially Blocks the Slow-Rising EPSC

The low-affinity antagonist kynurenic acid (Kyn) competes with glutamate during the rising phase of the AMPAR EPSC (Diamond and Jahr, 1997) and, thus, exerts a block whose magnitude is inversely related to transmitter concentration. We compared the effect of Kyn on the peak amplitude of the fast- and slow-rising EPSC to test whether they arose from different glutamate concentrations. Figure 4A shows that the two components of the EPSC were differentially blocked by Kyn. On average, Kyn (0.5–1 mM) produced a $50\% \pm 4\%$ ($n = 10$ cells) block of the peak of the fast-rising EPSCs. The slow-rising current was blocked by an additional $28\% \pm 5\%$ (Figure 4C). Preferential block of the EPSC at later times by Kyn can also be seen in the speeding of the mean EPSC waveform (Figure 4B), reducing the weighted decay by $27\% \pm 5\%$ on average ($n = 10$; Figure 4C) and was fully reversible in the three cells tested. During application of Kyn, there was no change in the paired pulse ratio, suggesting that release probability was unaffected (20–25 ms interval; $p = 0.68 \pm 0.07$, $n = 6$). When the mean EPSC amplitude was blocked to a similar degree by the noncompetitive antagonist GYKI 53655 ($44\% \pm 4\%$, $n = 10$; Kyn $43\% \pm 3\%$, $n = 11$; $p = 0.81$, unpaired t test) we saw neither a preferential block of the slow-rising events nor a change in the weighted decay (Figures 4D and 4E; $p = 0.17$ and $p = 0.25$, respectively). These results suggest that the AMPARs underlying the slow-rising events are exposed to a lower concentration of glutamate than those underlying the fast-rising component.

Lowering Release Probability Preferentially Reduces the Slow-Rising EPSCs

Lowering release probability reduces the level of interaction of transmitter released from neighboring release sites, and this can result in an acceleration in the decay

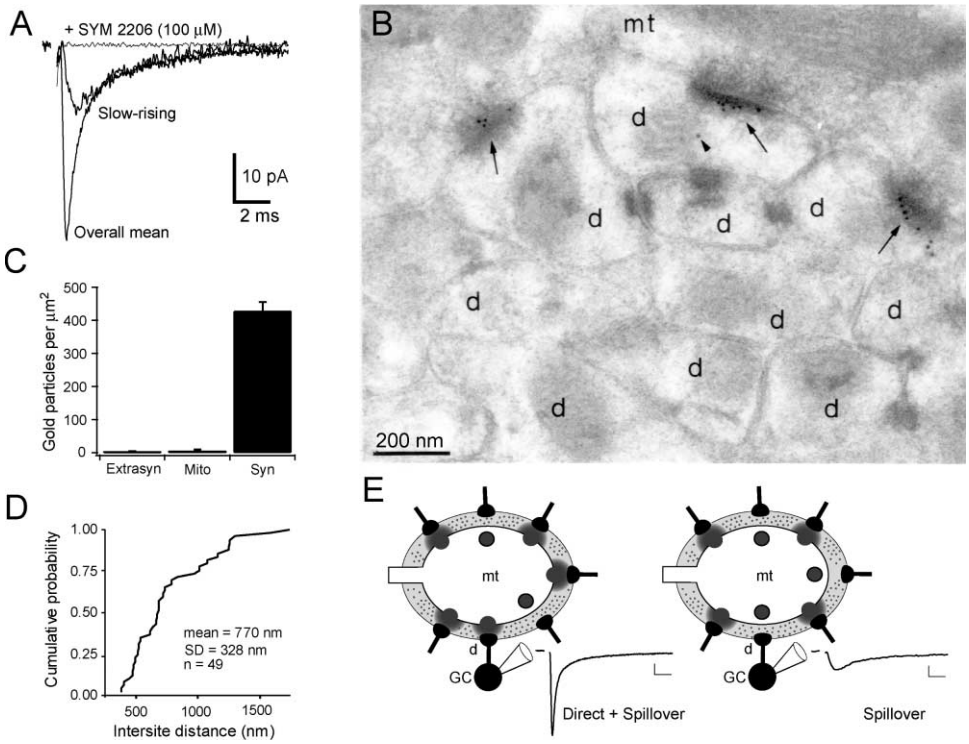

Figure 3. Fast- and Slow-Rising EPSCs Are Mediated by AMPARs Located Exclusively at the Synapse

(A) Overall mean EPSC and mean slow-rising EPSC before and after the addition of an AMPAR-specific antagonist SYM 2206 (thin trace).

(B) Electron micrograph showing immunogold localization of the GluR2/3/4c subunits in cerebellar glomeruli. Gold particles are concentrated in asymmetrical synaptic junctions (arrows) made by a mossy fiber terminal (mt) with granule cell dendrites (d). A single gold particle (arrowhead) was found over a mitochondrion. This is a single-sided reaction.

(C) Bar graph of the density of gold particles on mitochondria (Mito, i.e., background), extrasynaptic (Extrasyn), and synaptic (Syn) plasma membranes.

(D) Cumulative plot showing the distribution of edge-to-edge intersite distance measured from EMs.

(E) Schematic diagram illustrating the intersynaptic spillover hypothesis. Left side shows an MF terminal (mt) following a single AP when vesicles are released directly onto a PSDs located on a dendrite (d) of the granule cell (GC) from which we recorded. Lower concentrations of glutamate (gray dots) throughout the extracellular space are produced by vesicle fusions at AZs connecting to neighboring granule cells. The combined glutamate profile produces a fast-rising AMPAR-mediated EPSC with a slow-decaying current component (left trace). Right side, failure of direct release produces EPSC with a slow-rising and slow-decaying time course due solely to diffusion of glutamate from distant release sites.

Scale bar: 5 pA and 2 ms in (E).

of the mean EPSC (Hartzell et al., 1975; Mennerick and Zorumski, 1995; Otis et al., 1996; Silver et al., 1996b; Takahashi et al., 1995; Trussell et al., 1993). Figure 5A shows that the decay of the mean EPSC waveform at the MF-GC synapse accelerated when release probability was lowered (weighted decay 2.9, 2.3, and 1.9 ms with 2.0, 1.5, and 1.0 mM $[Ca^{2+}]_e$, respectively), suggesting that transmitter spillover is present. If the slow-rising events were mediated by spillover of glutamate from neighboring sites, their mean amplitude would be more sensitive to release probability than the peak amplitude of the overall mean EPSC, which occurs at a time when the fast-rising component predominates. Figure 5B illustrates such a preferential reduction in the amplitude of the slow-rising current relative to the overall mean as release probability was lowered (same cell as in Figure 5A). The weighted decay was reduced in 17 out of 19 connections with a reduction across all cells of 28% (2.5 $\pm$ 0.2 ms to 1.8 $\pm$ 0.2 ms; Figure 5C) and was reversible in the seven cells tested. The preferential reduction of slow-rising EPSCs was consistently observed as indicated by the decreased slow:all amplitude ratio (0.42 $\pm$ 0.06 to 0.23 $\pm$ 0.03, n = 10 cells; Figure 5C). The preferential sensitivity of the slow-rising component suggests that it arises from interaction of glutamate released from neighboring sites, consistent with our intersynaptic spillover hypothesis.

Amplitude Variability of Fast- and Slow-Rising Current Components

The spillover hypothesis predicts that slow-rising components arise from a larger number of release sites than the fast-rising current component and, thus, have a lower relative variability. Figure 6A shows a normalized mean EPSC and its corresponding normalized standard deviation (SD) for a connection with a robust slow-rising EPSC. The SD decayed well before the mean, indicating there was less variability associated with the slow-rising component than the fast-rising component. At a connection with negligible slow-rising currents, the SD and mean current decayed with similar time courses (Figure 6B). We quantified relative current fluctuations contrib-

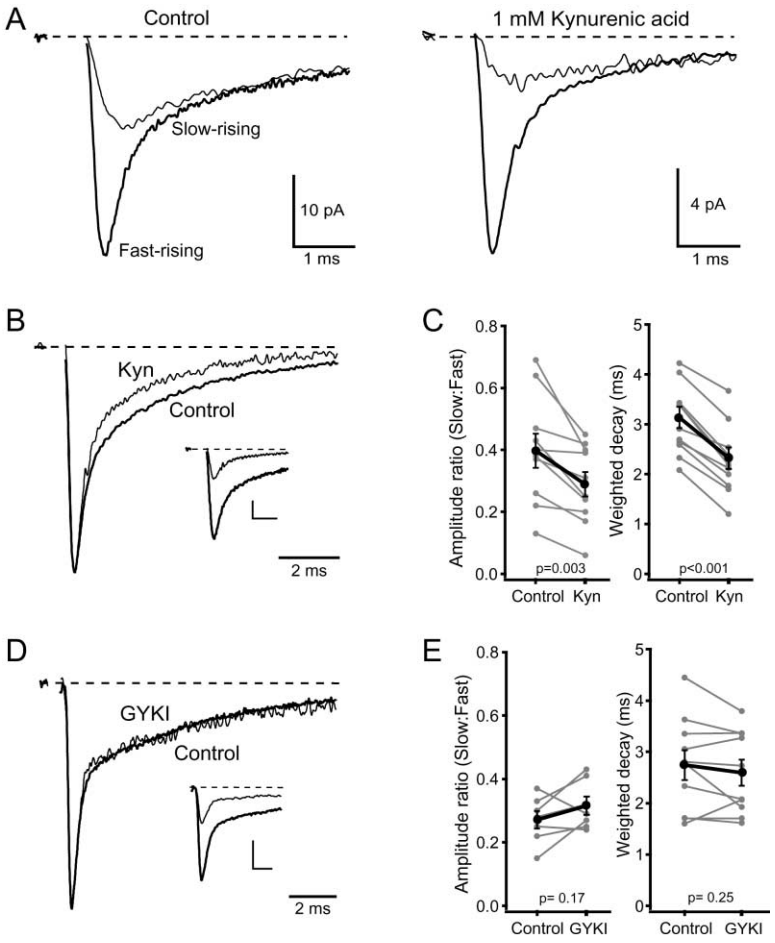

Figure 4. Low-Affinity Competitive Antagonist Preferentially Blocks Slow-Rising Events

(A) Mean fast- (thick trace) and slow-rising (thin trace) EPSCs under control conditions (left) and in the presence of kynurenic acid (Kyn) in the external solution (right).

(B) Normalized traces showing the acceleration of the overall mean EPSC from the same cell as in (A) in control (thick trace) and in the presence of 1 mM Kyn (thin trace). Inset, same traces as in (B), without normalization.

(C) Summary plots from several synaptic connections showing a reduction in the slow:fast amplitude ratio from 0.40 ± 0.05 to 0.29 ± 0.04 (n = 10, left) and an acceleration in the decay time course (weighted decay 3.1 ± 0.2 to 2.3 ± 0.2 ms, n = 10, right) in the presence of 0.5–1 mM Kyn.

(D) Normalized mean EPSCs recorded in control conditions (thick trace) and in the presence of a noncompetitive AMPAR-specific antagonist GYKI 53655 (2 μM, thin trace). Inset, raw averaged traces.

(E) Summary plots showing no preferential block of the slow-rising events (left, n = 7) and no change in the decay time course (right, n = 10) following the application of GYKI 53655.

Scale bar: 5 pA and 1 ms in (B) and (D).

uted by the slow-rising component by calculating the ratio of the coefficient of variation (CV = SD/mean) at the peak of the mean EPSC and 1 ms later, when the slow-rising current predominates. Figure 6C shows that there is a strong negative correlation between the weighted decay of the EPSC and the CV ratio, suggesting that cells with larger slow components exhibited relatively less variability in the EPSC at late times. Furthermore, reducing release probability, which preferentially reduces the amplitude of slow-rising EPSCs (see Figure 5), increased the CV ratio from 0.64 to 0.93 (1.0–1.25 mM $[Ca]_e$; $p < 0.01$; $n = 11$). These data are consistent with our hypothesis that the slow-rising currents arise from glutamate released from a larger number of release sites than those producing the fast component of the EPSC.

We calculated the relative number of release sites contributing to slow and fast components of the EPSC using the CV ratio. If release sites at a single terminal exhibit similar release probabilities, the CV of quantal release can be described as:

$$CV = \sqrt{\frac{1 - P}{NP}},$$

where N is the number of functional release sites and P is the mean release probability. Since P does not change as a function of time after the peak of the EPSC (see Experimental Procedures), the relative number of release sites at the peak and 1 ms later ($N_{1\ ms}/N_{peak}$) can be estimated without knowing P:

$$\frac{N_{1ms}}{N_{peak}} = \left(\frac{CV_{peak}}{CV_{1ms}}\right)^2.$$

Given the mean CV ratio of 0.6, we estimate that there are 2.8 times more release sites underlying the slow component of the EPSC than the fast component. After a correction for channel variance (see Experimental Procedures), this estimate N_{1ms}/N_{peak} increased to ~4. Error in the binomial estimate of N_{1ms}/N_{peak} could arise from the following synaptic parameters (Silver et al., 1998): (1) quantal variability at a single site, (2) variability in mean quantal size across sites, and (3) nonuniform release probability. These sources of variability, as well as contamination of the peak EPSC by spillover, will produce an underestimate of the relative number of release sites. Our estimate of $N_{1\ ms}/N_{peak}$ is, therefore, a lower limit and suggests that indirect sites are 3-fold more numerous.

Influence of Glutamate Uptake on the EPSC

We tested whether glutamate uptake limits spillover currents at the MF-GC synapse by examining the time course of the EPSC in the presence of uptake inhibitors. Application of 200 μM DL-TBOA, a noncompetitive in-

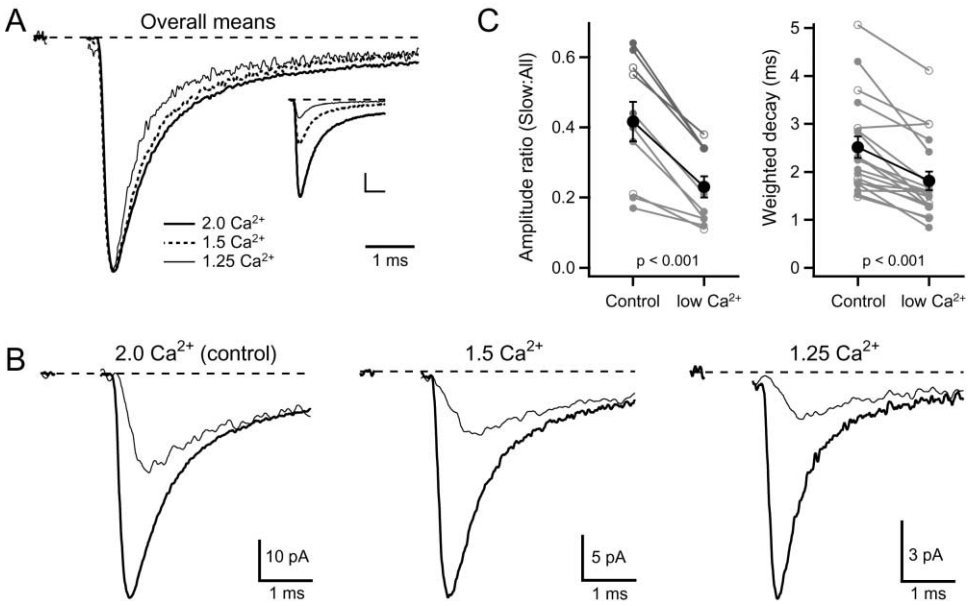

Figure 5. Lowering Release Probability Preferentially Reduces Slow-Rising EPSCs

(A) Comparison of normalized mean EPSC waveforms in 2 mM, 1.5 mM, and 1.25 mM $[Ca^{2+}]_e$. Inset, unscaled mean EPSCs.

(B) Overall mean (thick trace) and slow-rising mean (thin trace) EPSCs recorded from the same cell in 2 mM $[Ca^{2+}]_e$, (left), 1.5 mM (middle), and 1.25 mM (right).

(C) Summary plot of the ratio of the peak amplitude of the mean slow-rising EPSC to that of the overall mean (slow:all amplitude ratio) in control (2 mM) and low $[Ca^{2+}]_e$ (1.0–1.5 mM; left, n = 10), as well as the overall mean decay time course under these conditions (right, n = 19). Small, open symbols are data from cells in which the $[Ca^{2+}]_e$ was lowered to 1.5 mM, and the small, closed symbols correspond to that of 1.0 or 1.25 mM.

Scale bar: 10 pA and 1 ms in (A).

hibitor of glial and neuronal uptake (Shigeri et al., 2001; Shimamoto et al., 2000), had a small effect on the decay of single EPSCs (Figures 7A and 7C; 15% increase on average), consistent with previous studies in younger animals at room temperature (Sarantis et al., 1993). In six cells tested, there was no significant effect of TBOA on slow-rising EPSCs (Figure 7C). However, a much larger effect of TBOA was observed on the decay of the EPSC following a 100 Hz tetanic stimulation (Figures 7B and 7C; 60% on average; reversible to within 25% ± 15%, n = 7), similar to that previously reported at room temperature (Overstreet et al., 1999). The fact that uptake inhibitors had no detectable effect on isolated slow-rising events and only had a minor effect on the single EPSC suggests that glutamate uptake does not regulate glutamate spillover at early times.

Time Course and Charge Transfer of Direct and Spillover-Mediated EPSCs

In order to estimate the impact of the spillover current on AMPAR-mediated transmission, we calculated the overall mean, the spillover current component, and the direct release current component for the population (Figures 8A and 8B). The amplitude and time course of the direct release component was estimated in two ways: (1) from the mean of fast-rising EPSCs recorded under low release-probability conditions scaled to the peak of spillover-subtracted population mean (Figure 8B), and (2) by subtracting the scaled spillover waveform from the population mean waveform (Figure 8B). Table 1 summarizes the charge transfer and time course of each component. The scaled mean slow-rising current carried 70% of the charge of the overall mean EPSC (this represents an upper estimate, as summation is unlikely to be linear due to differences in receptor occupancy and/or desensitization when the direct release component is present). In contrast, the scaled mean fast-rising EPSC recorded in low $[Ca^{2+}]_e$, which accounted for 52% of the charge, provided a lower estimate of 48% (due to residual spillover, see Figure 5). We used this upper estimate of the direct release component to predict the relative impact of the individual current components on the EPSP.

Contribution of Spillover to the EPSP

We investigated how spillover currents contribute to the amplitude and time course of the EPSP by injecting the direct release and spillover conductance components (Figure 8C) into a passive model of the GC. Synaptic conductances were scaled by one third and injected into each of the three digits on a single dendrite, as for an input from a single MF terminal (Eccles et al., 1967). EPSPs generated with the direct release component had a rapid time to peak (t_{peak} = 1.2 ms) and rapid decay, with a half width of 4.8 ms (Figure 8D). The spillover component of the EPSP had a slower rise (t_{peak} = 3.5 ms) and decay (half width = 10.3 ms) than the direct release component, but the peak amplitude was only 22% smaller (direct = 5.9 mV, spillover = 4.6 mV). When the overall mean conductance waveform was injected,

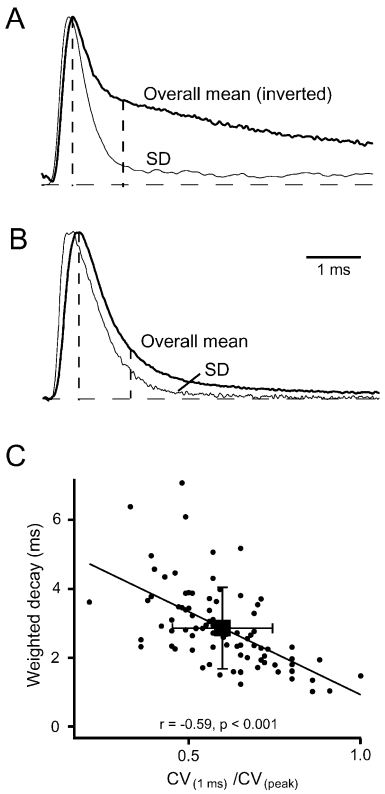

Figure 6. Reduction in the Variability during the EPSC Suggests an Increase in the Number of Release Sites with Time

(A) Inverted mean EPSC (thick trace) and its standard deviation (thin trace) recorded from a connection with a pronounced slow component. Vertical dashed lines indicate the locations where the coefficient of variation (CV) was calculated.

(B) Inverted mean EPSC (thick trace) and its standard deviation (thin trace) from a cell with a negligible slow-rising component.

(C) Summary plot showing that weighted decay correlates negatively with the ratio of the CV at 1 ms after the peak of the EPSC to that at the peak [$CV_{(1\ ms)}/CV_{(peak)}$]. On average, the $CV_{(peak)}$ was 0.52 $\pm$ 0.03, and $CV_{(1\ ms)}$ was 0.31 $\pm$ 0.02 (n = 86). The square is mean and SD of the weighted decay and CV ratio (2.9 $\pm$ 0.13 ms and 0.60 $\pm$ 0.14, respectively, n = 86 cells). The solid line is a linear fit.

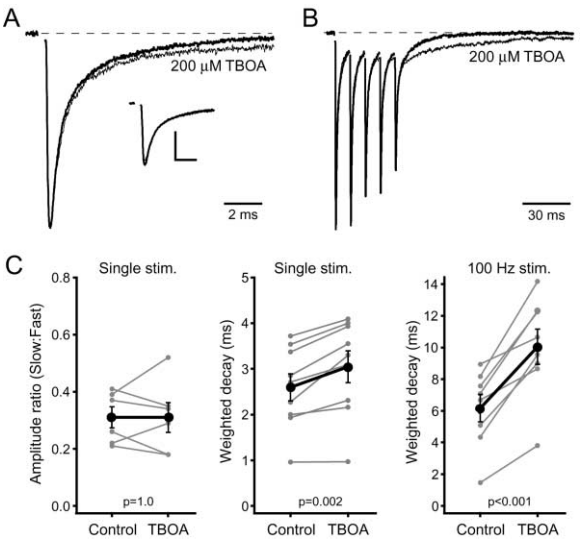

Figure 7. Glutamate Uptake Slows the EPSC at Late Times

(A) Mean EPSCs, recorded in response to a single stimulus at a synaptic connection with significant spillover component (slow:fast ratio is 0.37) under control conditions (thick trace) and in the presence of 200 μM of the glutamate uptake blocker TBOA (thin trace). Inset, raw mean traces show a small change in amplitude.

(B) Mean EPSCs from the same connection as in (A), but in response to a five pulse, 100 Hz stimuli.

(C) Summary plots showing that there was no significant change in the slow:fast amplitude ratio (left plot, 0.31 $\pm$ 0.04 versus 0.31 $\pm$ 0.05, n = 6) during application of 200 μM TBOA, however, there was a small increase in the decay time (middle plot, 2.6 $\pm$ 0.3 versus 3.0 $\pm$ 0.4 ms, n = 9) and a much larger increase weighted decay (integrated over 60 ms) following tetanic stimulation (right plot, 6.2 $\pm$ 0.9 versus 10.1 $\pm$ 1.1 ms, n = 9).

Scale bar: 20 pA, 2 ms in (A).

the simulations produced an EPSP amplitude of 7.5 mV, larger than that of the direct release component. The time to peak was slightly slower (t_{peak} = 1.6 ms), whereas the decay was much slower (half-width = 7.4 ms) than that of the direct release current component. These results indicate that the AMPAR conductance mediated by spillover is a major determinant of the EPSP waveform. Moreover, the impact of fluctuations in the amplitude of the highly variable direct release component will be limited by the spillover conductance, which is relatively invariant and rarely exhibits failures.

Discussion

We have shown that fast AMPAR EPSCs at the cerebellar MF-GC synapse are mediated by two independent components: a conventional fast-rising and -decaying current and a novel current with slower rising and decaying kinetics. Evidence from experiments using low-affinity antagonists, manipulations of release probability, and immunogold-labeling suggest that that slow-rising EPSCs result from activation of synaptic AMPARs by spillover of glutamate from AZs connected to neighboring cells. Fluctuation analysis indicates that these indirect release sites are at least 4-fold more numerous than those directly connected to the postsynaptic cell. The fact that spillover currents carry half the charge of the mean EPSC and are less variable suggests that spillover of glutamate plays an important role in fast synaptic transmission at this central synapse.

Other Possible Mechanisms that Could Produce the Slow-Rising Currents

It is possible that slow-rising currents could arise from the following unconventional release mechanisms: (1) full release of partially filled vesicles, and (2) slow release of glutamate through a nonexpanding fusion pore (Choi et al., 2000; Renger et al., 2001). The first possibility is unlikely because the rapid decay of neurotransmitter in the cleft (~100 μs decay; Clements, 1996) would produce fast-rising currents even if the glutamate concentration was initially low (Wahl et al., 1996). If the slowly rising events arose from prolonged glutamate release lasting over the time to the peak of the current, the decay in the glutamate concentration, when aligned at the start of release, would be faster than the decay in response to an instantaneous release (Choi et al., 2000).

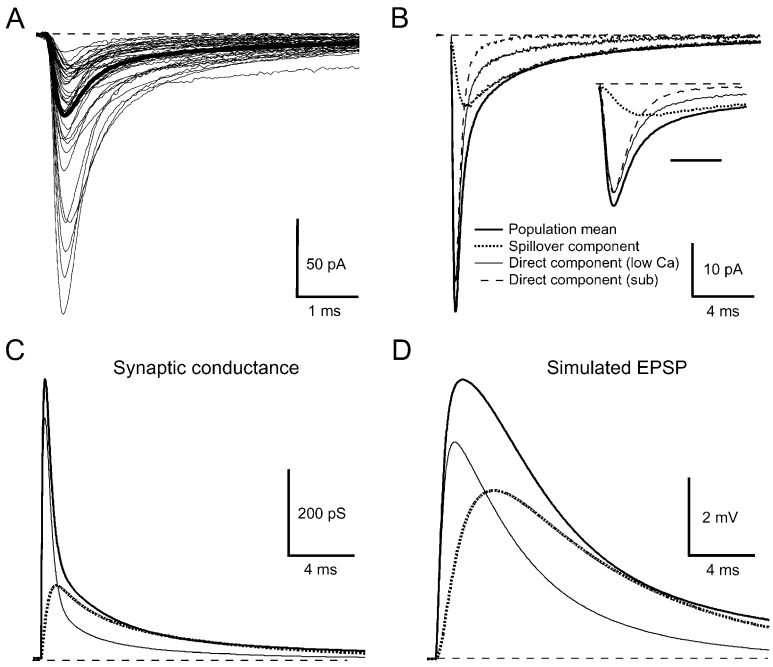

Figure 8. Spillover Currents Increase the Peak and Duration of Simulated EPSPs

(A) Individual mean traces (thin) from 38 synaptic connections and the population mean EPSC trace (thick).

(B) Population mean from (A) (thick trace), scaled population mean of slow-rising EPSCs (dotted trace, n = 20), the scaled population mean of the fast-rising EPSCs recorded in low $[Ca^{2+}]_e$ (thin trace, 1.0 or 1.25 mM $[Ca^{2+}]_e$, n = 13), and the difference between the population mean of all events and that of the scaled population mean of slow-rising EPSCs (dashed trace). The population mean slow-rising EPSC was scaled to the population mean at 5 ms (1.18×) since there was a significant difference between the EPSC amplitude from cells in which spillover currents were observed in isolation versus that of the entire population (35 ± 2 pA versus 47 ± 4 pA, n = 71 and n = 86, respectively; p = 0.01, unpaired t test), due to a lower release probability and/or fewer release sites. Inset, expanded time scale of population means.

(C) Direct release, spillover, and overall mean conductance waveforms estimated from multiexponential (one rising and three decaying) fits to the EPSC components in (B).

(D) Simulated EPSPs produced by conductance waveforms in (C) (resting potential of −75 mV). Legend for (B) also applies to (C) and (D).

Scale bar: 1 ms in (B).

We find that the slow-rising currents decay more slowly than the direct release component even after the fast component has decayed (Table 1, fit after 1.3 ms). Moreover, the preferential sensitivity of the slow-rising events to changes in release probability would not be expected for this mechanism. But it is still possible that a slow-rising and -decaying flux of glutamate is released into the cleft, a characteristic of immature and tetanus toxin-treated synapses (Renger et al., 2001). Such a release mechanism would have to be the most common release event to explain this result, which does not seem likely since slow-rising events were not observed at single site synapses in P12 GCs (Silver et al., 1996b).

A dependence of EPSC waveform on release probability and a lack of effect of uptake inhibitors have previously been interpreted as evidence for multivesicular release (Wadiche and Jahr, 2001). However, the fact that isolated spillover events are preferentially reduced when release probability is lowered argues against the possibility that the speeding of the EPSC decay is mediated solely by a reduction in multivesicular release from AZs. Our data would be consistent with multiple independent vesicles released outside the AZ if those vesicles exhibited a different $[Ca^{2+}]_e$ sensitivity to those released from within the AZ (due to a larger distance from Ca^{2+}-entry site). However, perisynaptic release of vesicles has not been reported and was not observed at single release site MF-GC connections in P12 animals (Silver et al., 1996b).

Slow-rising currents could potentially arise from a distinct population of synapses with AMPARs with slow kinetics and a higher sensitivity to Kyn, but to date, no such receptors have been described. Thus, the most parsimonious conclusion consistent with all the data

Table 1. Characteristics of the Population Mean EPSC and Its Underlying Current Components

	10%–90% Rise Time (ms)	Tau 1	Amp 1	Tau 2	Amp 2	Tau 3	Amp 3	Peak Amplitude (pA)	Charge (pC)	Weighted Decay (ms)	n
Population mean EPSC*	0.18	0.47	72%	4.5	23%	23.3	5%	54	128	2.4**	38
(fit from 1.3 ms*** after peak)				1.8	57%	11.0	43%				
Spillover EPSC	0.60	2.0	39%	9.1	61%			14	90	6.4	20
(fit from 1.3 ms after peak)				2.0	35%	9.0	65%				
Direct EPSC (low calcium)	0.20	0.39	83%	2.1	10%	6.8	7%	48	66	1.4	13
(fit from 1.3 ms after peak)				0.9	51%	5.9	49%				
Direct EPSC (subtracted)	0.16	0.37	94%	2.2	6%			48	38	0.8	

Multiexponential fits of EPSCs (Figure 8) were performed over a time extending 20 ms beyond the peak of the EPSC (except "*" 100 ms). The alignment of the individual mean slow-rising traces was on the 10% time point of its corresponding mean waveform. Note the weighted decay ("***") of the population mean for all cells (n = 86) was 2.9. ***1.3 ms corresponds to >3× the fast time constant of the isolated "direct" EPSC.

is that the isolated slow-rising events result from the spillover of transmitter from neighboring sites.

Mechanisms Underlying Release Probability-Dependent Changes in EPSC Waveform

Simple diffusion theory (i.e., without buffers) predicts that the glutamate concentration reached at a particular location is the linear sum of the concentrations arising from each source (Otis et al., 1996). The shape of the mean transmitter waveform at a particular location will therefore be independent of reductions in release probability if they occur uniformly across release sites. However, the mean concentration reached will be reduced. Changes in the mean glutamate waveform, rather than a simple scaling of its amplitude, would only be expected if the mean distance between releasing sites increases following a reduction in release probability (Mennerick and Zorumski, 1995; Silver et al., 1996b); but, a simple derivation shows that this is not the case (see Experimental Procedures). Glutamate transporters do not appear to play a significant role at the MF-GC synapse at early times ($\sim$1 ms), since TBOA does not affect the amplitude of the spillover component. Thus, a large part of the release probability-dependent changes in EPSC time course is likely to be due to nonlinearities of postsynaptic receptor activation (Faber and Korn, 1988; Hartzell et al., 1975) in response to the lower glutamate concentrations (Silver et al., 1996b) and/or other unidentified nonlinear aspects of glutamate diffusion (e.g., buffers).

Spillover onto AMPARs at Other Synapses

Rapid intersynaptic spillover ($<$1 ms rise time) onto AMPARs could be widespread in the CNS, but it may be difficult to assess its importance in shaping the EPSC waveform at other synapses. Spillover currents could contribute to EPSCs following release at boutons containing single AZs if a quantum of transmitter can activate receptors in multiple PSDs on the same cell. Unlike the case for the GC, such a spillover current would always be associated with a direct release component and the EPSC waveform would not change with release probability, making it difficult to identify. In preparations where isolated spillover currents occur, they may be difficult to identify since cable filtering by dendrites may prevent resolution of multiple populations of EPSC rise times on the submillisecond timescale.

Several factors influence the peak concentration of glutamate at neighboring release sites, including intersite distance, geometry, number of release sites, as well as the speed and location of glutamate uptake (Barbour and Hausser, 1997). The MF has many release sites located on the large continuous surface of the presynaptic terminal, while the postsynaptic dendrites are tightly packed and interconnected with numerous attachment plaques (Jakab and Hamori, 1988). Diffusion in this geometry is therefore likely to produce larger concentrations at neighboring release sites than predicted by a model that allows diffusion into a 3D space but less than that predicted from a simple disc model (Barbour and Hausser, 1997). The lack of a detectable effect of uptake inhibitors on the peak amplitude of slow-rising EPSCs and the lack of interdigitated glial cells suggests that uptake does not inhibit rapid intersynaptic diffusion of glutamate in the glomerulus.

Why have isolated AMPAR-mediated spillover currents not been described at this synapse in younger animals? Several developmental changes could underlie the appearance or increase in the spillover current component. Between P12 and P25, the anatomy of the glomerulus changes in several respects. The dendritic digits on which the synapses are located are short stubs at P12, but by P25, they differentiate into fingers several micrometers in length (Hamori and Somogyi, 1983). These changes may result in the nearest release sites being connected to the same GC at P12, but to different GCs at P25. Furthermore, during this period there is a 4-fold increase in the number of GC dendrites without a net increase in number of synaptic contacts (Hamori and Somogyi, 1983), suggesting that the number of contacts per dendrite decreases. This would produce an increase in the number of indirect release sites and, thus, could account for the more pronounced slow component of the EPSC in older animals (τ_{slow} = 6.0 ms, 11% in P12 (Silver et al., 1996a) versus τ_{slow} = 7.9 ms, 28% weighted average of τ_2 and τ_3, Table 1).

Glutamate spillover is likely to make the largest contribution to fast AMPAR EPSCs at connections that have multiple release sites in close proximity since this allows glutamate to summate sufficiently to activate receptors. Such examples include: MF synapses in the hippocampus, muscle spindle afferent boutons in the dorsal spinocerebellar tract, relay synapses in the auditory system, retinogeniculate synapses, climbing fiber synapses onto Purkinje cells, and synapses onto unipolar brush cells in cerebellum (Sheppard, 1998; Walmsley et al., 1998). Indeed, results from a deconvolution analysis that incorporated a diffusion model (Neher and Sakaba, 2001) suggest that slow-rising components of the AMPAR EPSCs are present at the calyx of held. Moreover, spillover may also contribute to the EPSC waveform in preparations where multiple closely spaced synaptic connections fire synchronously in vivo.

Physiological Implications

Three characteristics of the spillover component of AMPAR EPSCs are likely to be important in determining transmission properties at the MF-GC synapse: (1) its large charge transfer, (2) its release probability-dependent time course, and (3) its low variability. The spillover current component provides 48%–70% of the total charge transfer during the EPSC (Table 1). The spillover current, although slower than the direct component, is still fast enough to increase the peak amplitude of the EPSP. The increased amplitude and duration is likely to increase the reliability of transmission at this synapse and mean firing frequency for a given input frequency. Indeed, the presence of slow current components in the EPSC, such as those mediated by NMDA receptors, has been shown to increase the slope of input-output relationships (D'Angelo et al., 1995; Harsch and Robinson, 2000). The presence of the direct release component is likely to maintain temporal precision of EPSP-spike coupling (Fricker and Miles, 2000; Galarreta and Hestrin, 2001).

The high sensitivity of the spillover component to release probability suggests that the EPSC waveform and, thus, the EPSP amplitude and shape, will vary as a function of activity-dependent changes in release probability. At low MF-firing frequencies, the slightly slower spillover component would boost the quantal content of EPSPs such that threshold could be attained with fewer MF inputs. At higher firing frequencies, a condition where there is likely to be an activity-dependent reduction in release probability, a preferential reduction in the spillover component will accelerate the EPSP, thereby preserving action potential precision within the train. Under these conditions, the reduced boosting by the spillover component may be compensated for by temporal summation of EPSPs within the train, which will bring the membrane potential closer to firing threshold.

Synaptic connections with few release sites exhibit large trial-to-trial variability in EPSC amplitude at intermediate release probabilities, thus limiting transmission reliability. Transmission mediated by spillover of glutamate from neighboring sites may allow MFs to overcome these physical constraints by averaging over at least 4-fold more release sites. The low variability of the spillover component of the EPSC will reduce the variability in the peak amplitude of the EPSP by reducing or eliminating failures (see Figure 8D). Moreover, since other GCs can detect glutamate spillover, it may increase the chance that multiple GCs fire in synchrony (Maex and Schutter, 1998). Thus, AMPAR-mediated spillover currents at the MF synapse may be fast enough to improve the reliability of mapping MF activity onto the larger set of GCs. This enhanced information transfer at the input layer of the cerebellum may aid pattern separation in the cerebellar cortex (Marr, 1969; Tyrrell and Willshaw, 1992).

Experimental Procedures

Electrical Recording Conditions

Acute parasagittal slices of cerebellum were prepared from 24- to 26-day-old (25.0 ± 0.03, n = 86 cells) Sprague-Dawley rats as previously described (Silver et al., 1996b) except for the slicing solution, which contained 125 mM NaCl, 2.5 mM KCl, 2 mM $CaCl_2$, 1 mM $MgCl_2$, 1.25 mM NaH_2PO_4, 26 mM $NaHCO_3$, 25 mM glucose, and 1 mM Kyn (pH of 7.3). Recording solution was similar except that Kyn was omitted. For low $[Ca^{2+}]_e$ solutions, the $[Mg^{2+}]$ was increased such that solutions with 1.5, 1.25, and 1.0 mM Ca^{2+} contained 2.3, 3, and 3.7 mM Mg^{2+}, respectively. Patch electrodes contained 110 mM K-$MeSO_4$, 40 mM HEPES, 1 mM KCl, 4 mM NaCl, 0.5 mM EGTA, 0.3 mM NaGTP, and 4 mM MgATP (pH 7.3) and had resistances of 7–10 MΩ. Recordings were made at 35–39°C (37.3 ± 0.1, n = 86) in the presence of 10 μM AP5, 20 μM 7-chlorokynurenic acid, 10 μM SR-95531, and 0.5 μM strychnine to isolate non-NMDA receptor currents. GYKI 53655 was purchased from Sigma RBI and SYM 2206 and DL-TBOA from Tocris Cookson. EPSCs were elicited using minimal stimulation at ≤2 Hz and recorded using an Axopatch 200B amplifier at a holding voltage of −70 mV; liquid junction potentials were not corrected for. Currents were low-pass filtered with an 8-pole and 4-pole Bessel filter both with cutoff frequencies of 10 kHz. Signals were then digitized between 25–100 kHz with an ITC-18 interface using Axograph 4 software.

Amplitude and Rise Time Analysis

Data analysis was performed using custom software written in Igor Pro (Wavemetrics). Recordings were used for analysis if series resistances was <40 MΩ (uncompensated; 23.6 ± 0.5 MΩ in control conditions, n = 86), and the cell capacitance was <5 pF (2.70 ± 0.08 pF). EPSCs were baseline subtracted using a 0.5 ms window ~0.1 ms before the stimulus. EPSC amplitudes were estimated from five to ten point averages around the peak. All mean peak amplitudes and weighted decays were estimated from at least 60 stable events (except 100 Hz trains where at least 25 events were analyzed). EPSCs were analyzed if the amplitude of the stimulus artifact at the foot of the mean EPSC was <25% of the EPSC peak amplitude. In some cases, the stimulus artifact was subtracted by a double exponential fit to the mean failure trace or by subtracting scaled subthreshold traces. Individual events were denoted as synaptic failures if the mean value over a 1 ms window, including the peak of the mean EPSC, was smaller than three times the SD of mean background current calculated over a similar window, reflected in time about the midpoint of the baseline window.

Rise time analysis was performed on cells in which 75–350 EPSCs exhibited stable amplitudes (Spearman rank order correlation analysis; Silver et al., 1996b). Individual EPSCs were digitally low-pass filtered using a digital Gaussian filter with a cutoff frequency of 1.9–4 kHz to improve the accuracy of the rise time detection without significantly slowing fast-rising phase (<30 μs increase in 20%–80%). A 2–5 ms window was used to detect individual peak amplitudes from which either a 20%–80% or 30%–90% rise time was measured. Initial fitting parameters of the rise time distribution were selected using the automatic Igor routine, and the chi-squares were minimized using its Levenberg-Marquardt algorithm. EPSCs were considered as slow-rising if they were synaptic failures or if their measured rise times was greater than the mean + 5 × SD of a Gaussian fit to the rise time distribution (0.01 ms bin widths). All other EPSCs were grouped as fast-rising events. This procedure resulted in some currents with small fast-rising components ending up in the slow-rising group. We therefore applied a second criterion: when the derivative of the rise time was greater than 60–100 pA/ms (after 1.9 or 2.5 kHz filtering), currents were passed to the fast-rising group. Digital filter settings and thresholds for analysis remained identical before and after changes in external solutions.

Average 10%–90% rise times across cells were calculated from the unfiltered mean traces from connections in which the stimulus artifact contamination was <7% of the EPSC, and the corner frequency of the cell-electrode circuit was less than 1.5 kHz (mean 2.7 ± 0.1 kHz, n = 86). Mean EPSCs (elicited at ≤0.5 Hz) were aligned on the time point corresponding to 10% of the peak amplitude in order to estimate the population mean. Mean traces were presented as raw averaged traces, whereas mean slow-rising EPSCs were filtered up to a final 2.5 kHz cutoff frequency. The stimulus artifact was blanked for the presentation of mean traces. Values are stated as mean ± the standard error of the mean, unless otherwise noted. p values were determined using a paired Student's t test or a Pearson linear correlation test, unless stated otherwise. *r* is the Pearson coefficient.

Neurotransmitter release time course was estimated by fitting a Gaussian function (see Silver et al., 1996b) to the derivative of the rising phase of the overall mean (Figure 8). For calculation of the relative number of spillover sites, we corrected the measured CV^2 at the peak of the EPSC and 1 ms later by subtracting the CV^2 expected for 10 pS AMPAR channels (Silver et al., 1996b) at these two times. The corrected N_{1ms}/N_{peak} was 3.8–4.3 for the full range of possible channel open probabilities at the peak of the EPSC.

Postembedding Immunogold Localization of AMPA-Type GluRs

One 28- and two 34-day-old male Wistar rats were anaesthetized with Halothane and ketamine (400 mg/kg body weight) perfused through the heart first with 0.9% saline, then with a fixative containing 4% paraformaldehyde, 0.1% glutaraldehyde, and ~0.2% picric acid in 0.1 M phosphate buffer (pH = 7.4; PB) for 25–30 min. The brains were then removed, and blocks of cerebellar vermis were washed in PB. Vibratome sections (400–500 μm in thickness) were placed into 10%, 20%, and 30% glycerol in 0.1 M PB before they were plunged into −170 C° propane using a Leica EM CPC apparatus. The frozen sections were transferred to a freeze substitution apparatus (Leica EM AFS) where they were embedded in Lowicryl HM20 resin (Nusser et al., 1995). Postembedding immunogold reactions were carried out according to the method of Matsubara et al. (1996). Briefly, following Na-ethanolate and sodium borohydrate treatments, 2% bovine serum albumin (BSA) was used in Tris-buf-

fered saline with Triton X-100 for blocking and for diluting the primary and secondary antibodies. We used 5 μg/ml of the polyclonal rabbit anti-GluR2/3/4c antibody (Chemicon Int., Temecula, CA) and 10 μg/ml of the polyclonal rabbit anti-pan-AMPAR antibody (Nusser et al., 1998). The sections were incubated in the primary antibodies overnight, washed, then incubated in 10 nm gold-coupled goat anti-rabbit antibodies (British BioCell Intl., Cardiff, UK; 1:100 dilution) for 2 hr.

Quantification of the Immunogold Particles

Cerebellar glomeruli were photographed at a magnification of 20,000×. Images were digitized, and the total length of the extrasynaptic dendritic plasma membranes (average 70 μm/animal) and the postsynaptic membranes to MF terminals were measured using Scion Image 4.0.2 in at least four micrographs from each animal. The edges of the PSD were defined as the locations where electron-dense material disappeared. A gold particle was associated with the plasma membrane (both synaptic and extrasynaptic) if it was within 30 nm (Matsubara et al., 1996), resulting in an effective membrane width of 60 nm. The total membrane area was calculated from the total membrane length and from the effective membrane width, yielding a density measurement in gold particles/μm^2. Nonspecific labeling density was calculated (in gold particles/μm^2) from the total area of the mitochondria (as mitochondria do not have AMPARs) within the same images (3.7 μm^2 per animal) and from the number of gold particles.

Measurements of the Distance between the Nearest Neighboring Active Zones

A 29-day-old male Wistar rat was anaesthetized, perfused, and fixed as described above (but with 1.25% glutaraldehyde). Blocks from the vermis of the cerebellar cortex were embedded in Epoxi resin (Durcupan) using a standard procedure (Nusser et al., 1995). Ultrathin sections (70 nm in thickness) were cut and cerebellar glomeruli were randomly photographed at a magnification of 17,000×. The images were digitized, and the closest distance between asymmetrical MF to GC synapses was measured by following the plasma membranes in each micrograph using Scion Image 4.0.2.

EPSP Simulations

A passive model of the GC was constructed using the Neuron simulator (Hines and Carnevale, 1997). The morphology was as follows: soma diameter 7 μm; four dendrites of 13 μm length and 0.7 μm diameter; three dendritic digits per dendrite 3.2 μm in length and 0.4 μm in diameter; an unbranched axon of 100 μm length and 0.3 μm diameter (Eccles et al., 1967; Jakab and Hamori, 1988; Palay and Chan-Palay, 1974). This morphology had a capacitance of 2.4 pF assuming 1 $\mu F/cm^2$, close to the experimentally measured value. The specific membrane resistance (2430 Ωcm^2) was calculated from the membrane area of the model and input resistance at this age and temperature (1.0 ± 0.04 GΩ, n = 6; S.J.M. and A.S., unpublished data). The membrane potential was −75mV (Brickley et al., 2001) and axial resistivity assumed to be 150 Ωcm (Roth and Hausser, 2001). Conductance waveforms were calculated from multiexponential fits to the mean EPSC components (see Figure 8) after correcting for a junction potential (−10 mV).

Mathematical Relation between Mean Intersite Distance and Release Probability

The summed distances to sites that release transmitter ($\bar{l}$) averaged over n trials is given by

$$\bar{l} = \frac{1}{n}\sum_{i=1}^{n}\sum_{j=1}^{N} x_{ji}\rho_{ji},$$

where N is the total number of sites, x_{ji} is the distance to a particular site and ρ_{ji} is a random variable (0 or 1) that represents release at a particular site on a particular trial. Since the distance to each release site is constant across trials, then as $n \rightarrow \infty$ $\bar{l}$ simplifies to

$$\bar{l} = \sum_{j=1}^{N} x_j P_j,$$

where P_j is the release probability at a particular site. Since the mean number of sites that release transmitter per trial (quantal content) is N multiplied by the average release probability (P) and P_j is the same across all sites, the mean distance to releasing sites ($\bar{x}$) is,

$$\bar{x} = \frac{1}{NP}\sum_{j=1}^{N} x_j P = \frac{1}{N}\sum_{j=1}^{N} x_j.$$

Thus, $\bar{x}$ is independent of release probability.

Acknowledgments

This work was supported by the Wellcome Trust and European Commission. R.A.S. is in receipt of a Wellcome Senior Research Fellowship. Z.N. was supported by the Japan Science and Technology Corporation, the Hungarian Science Foundation (T032309), and the Howard Hughes Medical Institute. We thank D. Attwell, L. Cathala, S.J. Mitchell, and D. Rossi for helpful discussions during the project; D. Attwell for suggesting the derivation, S.J. Mitchell, J. Clements, and J. Rothman for software; and P. Somogyi for providing the anti-pan-AMPAR antibodies. We thank D. Attwell, L. Cathala, M. Farrant, S.J. Mitchell, T. Nielsen, and P. Sargent for their comments on the manuscript.

Received: March 19, 2002
Revised: June 25, 2002

References

Asztely, F., Erdemli, G., and Kullmann, D.M. (1997). Extrasynaptic glutamate spillover in the hippocampus: dependence on temperature and the role of active glutamate uptake. Neuron *18*, 281–293.

Barbour, B. (2001). An evaluation of synapse independence. J. Neurosci. *21*, 7969–7984.

Barbour, B., and Hausser, M. (1997). Intersynaptic diffusion of neurotransmitter. Trends Neurosci. *20*, 377–384.

Barbour, B., Keller, B.U., Llano, I., and Marty, A. (1994). Prolonged presence of glutamate during excitatory synaptic transmission to cerebellar Purkinje cells. Neuron *12*, 1331–1343.

Brickley, S.G., Revilla, V., Cull-Candy, S.G., Wisden, W., and Farrant, M. (2001). Adaptive regulation of neuronal excitability by a voltage-independent potassium conductance. Nature *409*, 88–92.

Bureau, I., Dieudonne, S., Coussen, F., and Mulle, C. (2000). Kainate receptor-mediated synaptic currents in cerebellar Golgi cells are not shaped by diffusion of glutamate. Proc. Natl. Acad. Sci. USA *97*, 6838–6843.

Carter, A.G., and Regehr, W.G. (2000). Prolonged synaptic currents and glutamate spillover at the parallel fiber to stellate cell synapse. J. Neurosci. *20*, 4423–4434.

Chen, S., and Diamond, J.S. (2002). Synaptically released glutamate activates extrasynaptic NMDA receptors on cells in the ganglion cell layer of rat retina. J. Neurosci. *22*, 2165–2173.

Choi, S., Klingauf, J., and Tsien, R.W. (2000). Postfusional regulation of cleft glutamate concentration during LTP at 'silent synapses'. Nat. Neurosci. *3*, 330–336.

Clements, J.D. (1996). Transmitter timecourse in the synaptic cleft: its role in central synaptic function. Trends Neurosci. *19*, 163–171.

D'Angelo, E., De Filippi, G., Rossi, P., and Taglietti, V. (1995). Synaptic excitation of individual rat cerebellar granule cells in situ: evidence for the role of NMDA receptors. J. Physiol. (Lond.) *484*, 397–413.

Diamond, J.S., and Jahr, C.E. (1997). Transporters buffer synaptically released glutamate on a submillisecond time scale. J. Neurosci. *17*, 4672–4687.

Eccles, J.C., Ito, M., and Szentagothai, J. (1967). The Cerebellum as a Computational Machine (Berlin: Springer-Verlag).

Faber, D.S., and Korn, H. (1988). Synergism at central synapses due to lateral diffusion of transmitter. Proc. Natl. Acad. Sci. USA *85*, 8708–8712.

Fricker, D., and Miles, R. (2000). EPSP amplification and the precision of spike timing in hippocampal neurons. Neuron *28*, 559–569.

Galarreta, M., and Hestrin, S. (2001). Spike transmission and syn-

chrony detection in networks of GABAergic interneurons. Science *292*, 2295–2299.

Geiger, J.R., Lubke, J., Roth, A., Frotscher, M., and Jonas, P. (1997). Submillisecond AMPA receptor-mediated signaling at a principal neuron-interneuron synapse. Neuron *18*, 1009–1023.

Hamori, J., and Somogyi, J. (1983). Differentiation of cerebellar mossy fiber synapses in the rat: a quantitative electron microscope study. J. Comp. Neurol. *220*, 365–377.

Harsch, A., and Robinson, H.P. (2000). Postsynaptic variability of firing in rat cortical neurons: the roles of input synchronization and synaptic NMDA receptor conductance. J. Neurosci. *20*, 6181–6192.

Hartzell, H.C., Kuffler, S.W., and Yoshikami, D. (1975). Post-synaptic potentiation: interaction between quanta of acetylcholine at the skeletal neuromuscular synapse. J. Physiol. (Lond.) *251*, 427–463.

Hausser, M., and Roth, A. (1997). Estimating the time course of the excitatory synaptic conductance in neocortical pyramidal cells using a novel voltage jump method. J. Neurosci. *17*, 7606–7625.

Hestrin, S. (1992). Activation and desensitization of glutamate-activated channels mediating fast excitatory synaptic currents in the visual cortex. Neuron *9*, 991–999.

Hines, M.L., and Carnevale, N.T. (1997). The NEURON simulation environment. Neural Comput. *9*, 1179–1209.

Isaacson, J.S. (1999). Glutamate spillover mediates excitatory transmission in the rat olfactory bulb. Neuron *23*, 377–384.

Jakab, R.L., and Hamori, J. (1988). Quantitative morphology and synaptology of cerebellar glomeruli in the rat. Anat. Embryol. (Berl.) *179*, 81–88.

Li, P., Wilding, T.J., Kim, S.J., Calejesan, A.A., Huettner, J.E., and Zhuo, M. (1999). Kainate-receptor-mediated sensory synaptic transmission in mammalian spinal cord. Nature *397*, 161–164.

Maex, R., and Schutter, E.D. (1998). Synchronization of golgi and granule cell firing in a detailed network model of the cerebellar granule cell layer. J. Neurophysiol. *80*, 2521–2537.

Marr, D. (1969). A theory of cerebellar cortex. J. Physiol. (Lond.) *202*, 437–470.

Matsubara, A., Laake, J.H., Davanger, S., Usami, S., and Ottersen, O.P. (1996). Organization of AMPA receptor subunits at a glutamate synapse: a quantitative immunogold analysis of hair cell synapses in the rat organ of Corti. J. Neurosci. *16*, 4457–4467.

Mennerick, S., and Zorumski, C.F. (1995). Presynaptic influence on the time course of fast excitatory synaptic currents in cultured hippocampal cells. J. Neurosci. *15*, 3178–3192.

Mitchell, S.J., and Silver, R.A. (2000). Glutamate spillover suppresses inhibition by activating presynaptic mGluRs. Nature *404*, 498–502.

Neher, E., and Sakaba, T. (2001). Combining deconvolution and noise analysis for the estimation of transmitter release rates at the calyx of held. J. Neurosci. *21*, 444–461.

Nusser, Z., Roberts, J.D., Baude, A., Richards, J.G., Sieghart, W., and Somogyi, P. (1995). Immunocytochemical localization of the alpha 1 and beta 2/3 subunits of the GABAA receptor in relation to specific GABAergic synapses in the dentate gyrus. Eur. J. Neurosci. *7*, 630–646.

Nusser, Z., Lujan, R., Laube, G., Roberts, J.D., Molnar, E., and Somogyi, P. (1998). Cell type and pathway dependence of synaptic AMPA receptor number and variability in the hippocampus. Neuron *21*, 545–559.

Otis, T.S., Wu, Y.C., and Trussell, L.O. (1996). Delayed clearance of transmitter and the role of glutamate transporters at synapses with multiple release sites. J. Neurosci. *16*, 1634–1644.

Overstreet, L.S., Kinney, G.A., Liu, Y.B., Billups, D., and Slater, N.T. (1999). Glutamate transporters contribute to the time course of synaptic transmission in cerebellar granule cells. J. Neurosci. *19*, 9663–9673.

Palay, S.L., and Chan-Palay, V. (1974). Cerebellar Cortex: Cortex and Organization (Berlin: Springer-Verlag).

Renger, J.J., Egles, C., and Liu, G. (2001). A developmental switch in neurotransmitter flux enhances synaptic efficacy by affecting AMPA receptor activation. Neuron *29*, 469–484.

Rossi, D.J., and Hamann, M. (1998). Spillover-mediated transmission at inhibitory synapses promoted by high affinity alpha6 subunit GABA(A) receptors and glomerular geometry. Neuron *20*, 783–795.

Roth, A., and Hausser, M. (2001). Compartmental models of rat cerebellar Purkinje cells based on simultaneous somatic and dendritic patch-clamp recordings. J. Physiol. (Lond.) *535*, 445–472.

Rusakov, D.A. (2001). The role of perisynaptic glial sheaths in glutamate spillover and extracellular Ca(2+) depletion. Biophys. J. *81*, 1947–1959.

Sarantis, M., Ballerini, L., Miller, B., Silver, R.A., Edwards, M., and Attwell, D. (1993). Glutamate uptake from the synaptic cleft does not shape the decay of the non-NMDA component of the synaptic current. Neuron *11*, 541–549.

Scanziani, M., Salin, P.A., Vogt, K.E., Malenka, R.C., and Nicoll, R.A. (1997). Use-dependent increases in glutamate concentration activate presynaptic metabotropic glutamate receptors. Nature *385*, 630–634.

Sheppard, G.M. (1998). The Synaptic Organization of the Brain, Fourth Edition (New York: Oxford University Press).

Shigeri, Y., Shimamoto, K., Yasuda-Kamatani, Y., Seal, R.P., Yumoto, N., Nakajima, T., and Amara, S.G. (2001). Effects of threo-beta-hydroxyaspartate derivatives on excitatory amino acid transporters (EAAT4 and EAAT5). J. Neurochem. *79*, 297–302.

Shimamoto, K., Shigeri, Y., Yasuda-Kamatani, Y., Lebrun, B., Yumoto, N., and Nakajima, T. (2000). Syntheses of optically pure beta-hydroxyaspartate derivatives as glutamate transporter blockers. Bioorg. Med. Chem. Lett. *10*, 2407–2410.

Silver, R.A., Traynelis, S.F., and Cull-Candy, S.G. (1992). Rapid-time-course miniature and evoked excitatory currents at cerebellar synapses in situ. Nature *355*, 163–166.

Silver, R.A., Colquhoun, D., Cull-Candy, S.G., and Edmonds, B. (1996a). Deactivation and desensitization of non-NMDA receptors in patches and the time course of EPSCs in rat cerebellar granule cells. J. Physiol. (Lond.) *493*, 167–173.

Silver, R.A., Cull-Candy, S.G., and Takahashi, T. (1996b). Non-NMDA glutamate receptor occupancy and open probability at a rat cerebellar synapse with single and multiple release sites. J. Physiol. (Lond.) *494*, 231–250.

Silver, R.A., Momiyama, A., and Cull-Candy, S.G. (1998). Locus of frequency-dependent depression identified with multiple-probability fluctuation analysis at rat climbing fibre-Purkinje cell synapses. J. Physiol. (Lond.) *510*, 881–902.

Smith, T.C., Wang, L.Y., and Howe, J.R. (1999). Distinct kainate receptor phenotypes in immature and mature mouse cerebellar granule cells. J. Physiol. (Lond.) *517*, 51–58.

Takahashi, M., Kovalchuk, Y., and Attwell, D. (1995). Pre- and post-synaptic determinants of EPSC waveform at cerebellar climbing fiber and parallel fiber to Purkinje cell synapses. J. Neurosci. *15*, 5693–5702.

Trussell, L.O., Zhang, S., and Raman, I.M. (1993). Desensitization of AMPA receptors upon multiquantal neurotransmitter release. Neuron *10*, 1185–1196.

Tyrrell, T., and Willshaw, D. (1992). Cerebellar cortex: its simulation and the relevance of Marr's theory. Philos. Trans. R. Soc. Lond. B Biol. Sci. *336*, 239–257.

Wadiche, J.I., and Jahr, C.E. (2001). Multivesicular release at climbing fiber-Purkinje cell synapses. Neuron *32*, 301–313.

Wahl, L.M., Pouzat, C., and Stratford, K.J. (1996). Monte Carlo simulation of fast excitatory synaptic transmission at a hippocampal synapse. J. Neurophysiol. *75*, 597–608.

Walmsley, B., Alvarez, F.J., and Fyffe, R.E. (1998). Diversity of structure and function at mammalian central synapses. Trends Neurosci. *21*, 81–88.

Wilding, T.J., and Huettner, J.E. (1995). Differential antagonism of alpha-amino-3-hydroxy-5-methyl-4- isoxazolepropionic acid-preferring and kainate-preferring receptors by 2,3-benzodiazepines. Mol. Pharmacol. *47*, 582–587.